Comparison of two remote sensing models for estimating evapotranspiration: algorithm evaluation and application in seasonally arid ecosystems in South Africa

Sebinasi DZIKITI[1*], Nebo Z JOVANOVIC[1], Richard DH BUGAN[1], Abel RAMOELO[2], Nobuhle P MAJOZI[2], Alecia NICKLESS[2], Moses A CHO[2], David C LE MAITRE[1], Zanele NTSHIDI[1], Harrison H PIENAAR[1]

[1] Council for Scientific and Industrial Research, Natural Resources and Environment, Stellenbosch 7599, South Africa;
[2] Council for Scientific and Industrial Research, Natural Resources and Environment, Pretoria 0001, South Africa

Abstract: Remote sensing tools are becoming increasingly important for providing spatial information on water use by different ecosystems. Despite significant advances in remote sensing based evapotranspiration (ET) models in recent years, important information gaps still exist on the accuracy of the models particularly in arid and semi-arid environments. In this study, we evaluated the Penman-Monteith based MOD16 and the modified Priestley-Taylor (PT-JPL) models at the daily time step against three measured ET datasets. We used data from two summer and one winter rainfall sites in South Africa. One site was dominated by native broad leaf and the other by fine leafed deciduous savanna tree species and C_4 grasses. The third site was in the winter rainfall Cape region and had shrubby fynbos vegetation. Actual ET was measured using open-path eddy covariance systems at the summer rainfall sites while a surface energy balance system utilizing the large aperture boundary layer scintillometer was used in the Cape. Model performance varied between sites and between years with the worst estimates ($R^2<0.50$ and RMSE>0.80 mm/d) observed during years with prolonged mid-summer dry spells in the summer rainfall areas. Sensitivity tests on MOD16 showed that the leaf area index, surface conductance and radiation budget parameters had the largest effect on simulated ET. MOD16 ET predictions were improved by: (1) reformulating the emissivity expressions in the net radiation equation; (2) incorporating representative surface conductance values; and (3) including a soil moisture stress function in the transpiration sub-model. Implementing these changes increased the accuracy of MOD16 daily ET predictions at all sites. However, similar adjustments to the PT-JPL model yielded minimal improvements. We conclude that the MOD16 ET model has the potential to accurately predict water use in arid environments provided soil water stress and accurate biome-specific parameters are incorporated.

Keywords: MOD16 ET; drought stress; model validation; Penman-Monteith; Priestley-Taylor; sensitivity analysis

1 Introduction

Effective management of water resources in arid and semi-arid environments requires accurate tools to quantify key components of the hydrological cycle such as the evapotranspiration (ET). More than 70% of precipitation received in arid environments is returned to the atmosphere via ET annually (Zhang et al., 2016; Dzikiti et al., 2018). Consequently, ET is a major component in the processes and models of climate change, water balance, groundwater recharge, net primary productivity, floods, droughts and irrigation (Fisher et al., 2008; Műnch et al., 2013). It is also the most difficult and complicated component to measure and predict because of the heterogeneity in the landscape and the large number of controlling factors which include climate, plant biophysics, soil properties and topography (Dzikiti et al., 2016; El Masri et al., 2019). Typically modelled ET data show uncertainties in the range of 15%–30% (Velpuri et al., 2013; Garcia et al., 2014). However, the errors can be as high as 50% or more in arid and semi-arid environments (Garcia et al., 2013).

Physically based models of ET that use the combination Penman-Monteith (PM) approach have been evaluated in recent years using a range of satellite products (Nishida et al., 2003; Cleugh et al., 2007; Mu et al., 2007; Mu et al., 2011; Ershadi et al., 2014; Talsma et al., 2018; El Masri et al., 2019). The models range in complexity from simple single source models (Cleugh et al., 2007; Ershadi et al., 2014) to dual source models (Mu et al., 2007; Talsma et al., 2018; El Masri et al., 2019) and to more complex multi-source models (Mu et al., 2011, 2013). The ET model by Mu et al. (2007) that used remote sensing inputs from the moderate resolution imaging spectrometer (MOD16), was initially a dual source model. In this model ET was calculated as the algebraic sum of evaporation from the bare soil and transpiration from plant canopies. In recent years, MOD16 has evolved into a multi-source PM based model, a culmination of numerous improvements that have occurred over the years. According to Mu et al. (2011, 2013), MOD16 ET is calculated as the sum of evaporation from wet canopy surfaces, plant transpiration, and evaporation from the wet and dry soil surfaces. In addition, all the fluxes are computed for both day and night time periods. Globally ET estimates over vegetated land surfaces are now operationally produced at 1-km^2 resolution using data from the moderate resolution imaging spectrometer and the MOD16 algorithm (Ruhoff et al., 2013). Examples of the application of this tool include groundwater recharge estimates in the dry Sandveld region of South Africa (Műnch et al., 2013) and for quantifying water use by agricultural crops in Brazil (Ruhoff et al., 2013).

Another remote sensing ET model that has been the subject of extensive research is the radiation based Priestley-Taylor model (Priestley and Taylor, 1972) modified by the Jet Propulsion Laboratory at NASA (PT-JPL; Fisher et al., 2008; Yao et al., 2013; Yao et al., 2015). A key advantage of the PT-JPL over the MOD16 model is that it requires less input variables. Large amounts of input data lead to an accumulation of errors which magnify the uncertainties in ET predictions. Some studies have in fact, reported higher accuracy with the PT-JPL (Garcia et al., 2013; Ershadi et al., 2014). Furthermore, the PT-JPL avoids the calculation of the aerodynamic and surface resistances thus substantially simplifying the model. A common weakness of most remote sensing ET models however, is that results at dry sites tend to be less accurate than at more humid sites (Zhang et al., 2008, 2010; Marshall et al., 2013; Mu et al., 2013; Polhamus et al., 2013). A possible reason for the loss of accuracy is the difficulty in parameterizing the soil-plant-atmosphere interactions and other biophysical constraints under arid conditions where latent heat fluxes are relatively low especially under sparse vegetation cover. Consequently, more data and improved parameterization of the ET models remain a priority in arid and semi-arid environments where these tools are most needed for water resources management.

The aims of this study were firstly to compare the performance of two widely used remote sensing ET models (i.e., MOD16 and PT-JPL) using actual ET measurements from semi-arid sites with contrasting vegetation characteristics in South Africa. Secondly, improvements to the models were proposed and the models were validated using *in situ* ET measurements. Besides the work by El Masri et al. (2019) in China and Mu et al. (2013) in the Nile valley, few studies have focused on the physics of the MOD16 model using daily data from seasonally arid ecosystems. We used soil,

plant and atmospheric data from deciduous broad and fine leafed native savannas with C_4 grasses found in most parts of summer (October–March) rainfall region in Southern Africa. These savannas are prone to long mid-summer dry spells often lasting several weeks to months (Makarau and Jury, 1997). This unavoidably induces severe water stress during the active transpiration period and we sought to establish how the ET models can be improved under these conditions. The other data was collected in the fynbos biome, a sclerophyllous shrub dominated by species of the Proteaceae, Ericaceae, and Restionaceae (Low and Rebelo, 1996) found in the winter (May–August) rainfall Cape Floral Region of South Africa. Model simulations were compared with field data collected using eddy covariance systems and an energy balance approach that combined sensible heat flux data collected using a large aperture boundary layer scintillometer with net radiation and soil heat flux measurements.

2   Materials and methods

2.1   Study area

South Africa hosts several climatic zones within its borders (Schulze et al., 2008). These are determined by the country's location in the Southern Hemisphere's subtropics (22°–35°S) and between the two oceans of the Atlantic to the west and the Indian Ocean to the east. The northeastern parts of the country have a predominantly humid subtropical climate (Fig. 1). These regions receive summer rainfall between October and March the next year. The southwestern corner (the Cape region) has a Mediterranean type climate with most rain falling in winter between May and August. Vegetation in these regions reflects the prevailing climatic and edaphic conditions. Data used in this study were collected in three seasonally arid biomes with native vegetation namely Skukuza, Malopeni and Elandsberg. A summary of the prevailing conditions at each site is given in Table 1.

Table 1   Characteristics of the study sites

Site	Location	Climatic region	Temperature	Rainfall (mm/a)	Vegetation characteristics
Skukuza	25°12′S, 31°30′E	Summer rainfall (Oct–Mar)	14.5°C–29.5°C	547	Mixture of tall (>9.0 m) broad-leafed Combretum savanna and fine-leafed *Acacia* savanna. Approx. 20%–40% canopy cover.
Malopeni	23°50′S, 31°13′E	Summer rainfall (Oct–Mar)	12.0°C–30.5°C	472	Hot and dry savanna vegetation dominated by short (<5.0 m) broad-leafed *Colophospermum mopane* vegetation. Approx. 15%–40% canopy cover.
Elandsberg	33°28′S, 19°04′E	Winter rainfall (May–Aug)	9.0°C–35.0°C	600	Shrubby fynbos dominated by 0.7–0.9 m small leaved proteoid shrubs and reed-like restiods. Approx. 20%–50% canopy cover.

2.1.1   Skukuza

The Skukuza site was located in a semi-arid region with subtropical climatic conditions in South Africa (Fig. 1). This site was established in 2000 and full details can be found in Scholes et al. (2001). The site is situated within the greater Kruger National Park, a 2×10^6 hm^2 game reserve located in the northeastern part of the country. Vegetation consisted of the Granite Lowveld vegetation type according to the classification by Mucina and Rutherford (2006). This comprised a mixed lowland bushveld with elements of the "Legogote Sour Bushveld" typical of the savanna biome. Mean tree height was around 9.0 m with a tree density of about 128 stems/hm^2 (Scholes et al., 2001). Dominant tree species included the *Combretum apiculatum*, *Terminalia sericea*, *Sclerocarya birrea*, and *Senegalia nigrescens*, among others. A perennial grass layer formed most of the basal cover dominated by the *Panicum maximum* and *Digitaria erianthia* species. The site had both broad and fine-leaved savanna with a long-term mean annual rainfall of about 547 mm. So the location of the flux tower allowed ET from the different savanna types to be quantified.
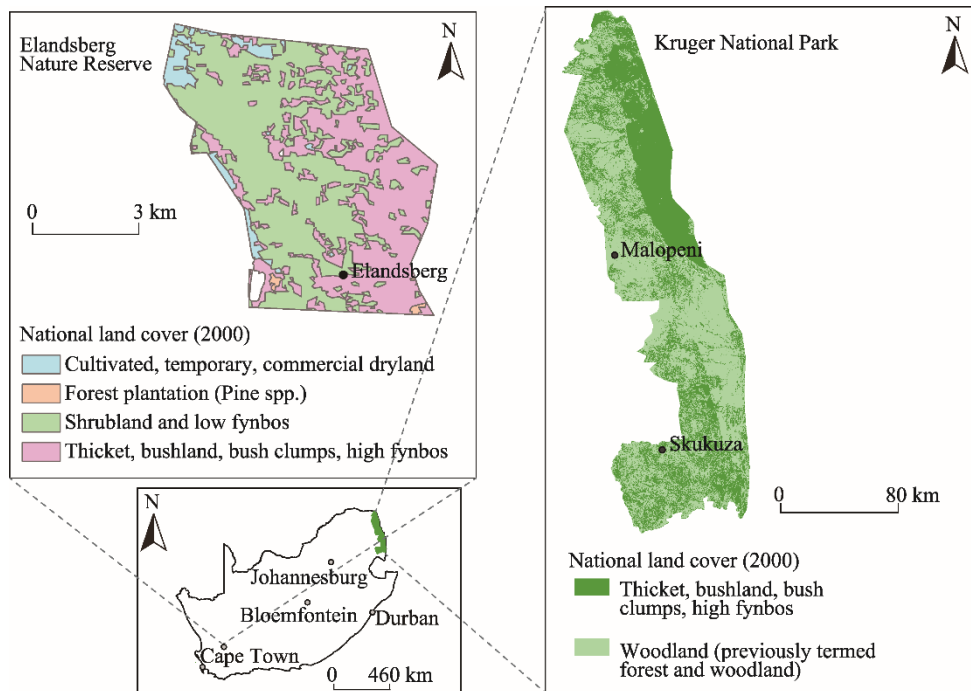
Fig. 1   Location of the study sites: Skukuza, Malopeni and Elandsberg and the associated vegetation types derived from the national land cover map of 2000

2.1.2   Malopeni

The Malopeni flux tower was located at the northern part of Kruger National Park (Fig. 1), dominated by the broad-leaf *Cholophospermum mopane*, a typical species of hot and dry savannas found in low-lying regions of Southern Africa. The dominant grass species was *Panicum maximum* while *mopane* trees made up more than half of the tree composition at the site. The average tree height was approximately 5.3 m and tree density was about 828 stems/hm^2. The average temperature ranged from 12.4°C to 30.5°C with the maximum temperature reaching up to 45.0°C in the hot summer months (October–March). Minimum temperatures seldom dropped to below 5.0°C, even during winter. The soils were shallow sandy loam luvisol formed from a base of Archaean granites and gneisses (Cleverly and Bristow, 1979), with a depth of less than 40 cm.

2.1.3   Elandsberg

The Elandsberg site was situated in a 2000 hm^2 nature reserve on the west-facing foot slopes of the Elandskloof mountain range in the Western Cape Province of South Africa (Fig. 1). A detailed description of the site is given by Dzikiti et al. (2014). The dominant vegetation type was the Swartland alluvial fynbos (Mucina and Rutherford, 2006) on deeper sandy soils interspersed with patches of Swartland shale renosterveld on more stony, shale-derived soils. The Swartland alluvial fynbos was dominated by 0.7–0.9 m tall, small-leaved proteoid shrubs, with a lower layer of fine leafed shrubs and reed-like restioids. Where the shale was exposed, renosterveld vegetation replaced the fynbos. In the shallow stream valleys sandy, alluvial soils have accumulated which, together with the additional moisture supported a community which had a greater cover of sedges and grasses than the adjacent dry land fynbos. The climate at Elandsberg was Mediterranean type with rain falling during winter (May–August).

2.2   Measurements of evapotranspiration (ET), weather and ancillary data

2.2.1   Skukuza and Malopeni

Actual ET was measured at Skukuza and Malopeni using open path eddy covariance systems mounted on towers. We used two years' data for Skukuza collected from January 2010 to December 2011 for this study. This time span was sufficiently long given that we used daily ET data for our

assessments. For Malopeni, we used data from February 2009 to March 2010 which were the only available data. The eddy covariance equipment at Skukuza comprised a 3-D sonic anemometer (CSAT-3, Campbell Scientific, Inc., Logan, UT, USA) and an infrared gas analyser (LI-7500; Li-Cor, Lincoln, Nebraska, USA) all installed at a height of about 16 m above the ground with a flux footprint of about 700 m around the tower considering the fact that the fetch of the eddy covariance system increases by about 100 m for every 1.0 m above the mean canopy height. At Malopeni, another 3-D sonic anemometer (Gill WindMaster Pro, Gill Instruments, Lymington, UK) was installed together with a LI-7500 infrared gas analyser and the instruments were mounted at 7 m height with a flux footprint of around 300 m radius. The 3-D wind speed (u, v, w) and water vapour concentration were sampled at 20 Hz frequency and the outputs processed at 30 min intervals. Post-processing of the high frequency data was done including coordinate rotations, corrections for air density fluctuations, de-spiking, etc. using the EddyPro software (EddyPro v 6.2.0; Li-Cor, Lincoln, Nebraska, USA), to ensure good quality ET measurements (Burba and Verma, 2005). At both sites, the eddy-covariance data were logged using data-loggers (CR3000; Campbell Scientific, Inc., Logan, UT, USA).

Available energy data (net radiation-soil heat flux) were collected at both sites using net radiometers (NR-Lite, Kipp & Zonen, Delft, The Netherlands) mounted on the flux towers and soil heat flux plates (HFT3; Campbell Scientific, Inc., Logan UT, USA) installed at depths of 50 and 700 mm at Skukuza and 80 mm at Malopeni near the flux towers. Volumetric soil water content was measured using water content reflectometers (CS615; Campbell Scientific, Inc., Logan UT, USA) at 50, 130, 290 and 610 mm depths at Skukuza and using EC-5 (Decagon Devices, Pullman, WA, USA) sensors at 50, 150, 250 and 350 mm depths at Malopeni. Climate data were measured using automatic weather stations installed on the flux towers. Temperature and relative humidity were monitored using HMP50 sensors (Vaisala, Helsinki, Finland), rainfall with tipping bucket rain gauges (TE525-M; Campbell Scientific, Inc., Logan UT, USA), wind speed and direction with wind sentries (03001, R.M. Young; Campbell Scientific, Inc., Logan UT, USA), and photosynthetically active radiation (PAR) with quantum sensors (Li-190; Li-Cor, Lincoln, Nebraska, USA). All sensors were installed at a height of 16 m, except for the rain gauge and wind sensor which were placed at 22 m at Skukuza and at 5 m at Malopeni.

2.2.2 Elandsberg

Climate, soil water content and actual ET data were collected from November 2012 to October 2013. Weather data were collected using an automatic weather station which measured the temperature and relative humidity using a temperature and humidity probe (CS500; Vaisala, Finland). Wind speed and direction were measured using a wind sentry (03001, R.M. Young; Campbell Scientific, Inc., Logan, USA) installed at 2.0 m height while the solar irradiance was measured using a pyranometer (SP 212; Apogee Instruments, Inc., Logan UT, USA). Rainfall was monitored using a tipping bucket rain gauge (TE525-L; Campbell Scientific, Inc., Logan UT, USA). Net radiation at the surface was measured using a net radiometer (CNR 1; Kipp & Zonen, Delft, The Netherlands) mounted at a height of 2.5 m above the ground while the soil heat flux (G) was measured using a cluster of four soil heat flux plates (REBS, Inc., Seattle, WA, USA) installed at 80 mm depth at different locations within the study area. To correct for the heat stored above the soil heat flux plates, we measured the soil temperatures at 20 and 60 mm depth, respectively, using the soil averaging thermocouples (TCAV-L; Campbell Scientific, Inc., Logan UT, USA) while the soil water content was measured using water content reflectometers (CS616; Campbell Scientific, Inc., Logan UT, USA). All the sensors were connected to a data logger (CR23X; Campbell Scientific, Inc., Logan UT, USA) programmed with a scan interval of 10 s and all the outputs were processed every 30 min.

Latent heat flux, which is the energy equivalent of actual ET (λE, in W/m^2) was determined using the shortened surface energy balance equation (Monteith and Unsworth, 1990) in which:

$$\lambda E = R_n - G - H \, , \tag{1}$$

where E is the evaporation rate (kg/(m$^2 \cdot$s)); R_n is the net radiation (W/m^2); G is the soil heat flux

(W/m^2); H is the sensible heat flux (W/m^2); and λ is the latent heat of vaporization (J/kg). The sensible heat flux component was measured using the large aperture boundary layer scintillometer (Model: BLS 900, Scintec, AG, Germany). The scintillometer measures changes in the refractive index of the air between a transmitter of monochromatic infrared radiation (880 nm; 33°28′13″S, 19°03′29″E; 152 m a.s.l.) and a receiver (33°28′27″S, 19°03′46″E; 157 m a.s.l.). The distance between the scintillometer transmitter and receiver was about 1000 m. Effective height of the scintillometer beam above the ground was about 4.8 m and this was calculated using detailed transect elevation and vegetation height data according to the approach by Savage et al. (2004). Measurements were taken within a 1 km^2 area that matched a MOD16 pixel. The fewer points at Elandsberg were a result of loss of data due to power failure to the scintillometer.

2.3 Remote sensing data

MODIS Terra 1 km data products were used as inputs for the simulations. These included the 8-d fraction of the photosynthetically active radiation (FAPAR) and leaf area index (LAI, ratio of leaf area to ground area; m^2/m^2), MCD15A2; 16-d surface albedo, MCD43C1; and 16-d normalised difference vegetation index (NDVI), MCD13A2. These data were downloaded from the Land Processes Distributed Active Archive Centre of the United States (http://lpdaac.usgs.gov). The data for each study site were extracted for each input, and interpolated linearly to obtain the daily values. The FAPAR was used a surrogate for the fractional vegetation cover according to Mu et al. (2011). So we assumed a constant value over the 8-d period.

2.4 Model improvements

A detailed description of the MOD16 model is given by Mu et al. (2011). Here the focus is on changes that improved the performance of MOD16 at the semi-arid sites. According to the PM equation, the latent heat flux (λE (W/m^2)) is calculated as:

$$\lambda E = \frac{\Delta A + \rho C_p (e_{\text{sat}} - e_a) / r_a}{\Delta + \gamma (1 + r_s / r_a)}, \tag{2}$$

Where λ is the latent heat of vaporization (J/kg); Δ is the slope of the saturation vapour pressure-temperature curve (kPa/K); A is the available energy at the given surface (W/m^2); ρ is the density of air (kg/m^3); C_p is the specific heat capacity of air at constant pressure (J/(kg·K)); e_{sat} is the saturated vapour pressure; e_a is the actual vapour pressure of the air (kPa); r_a is the aerodynamic resistance (s/m); γ is the psychrometric constant (kPa/K); and r_s is the surface resistance (s/m). Mu et al. (2011) defined A as:

$$A = R_n, \tag{3}$$

where R_n is the net radiation absorbed by the surface. This equation assumes that the soil heat flux is negligible. The R_n is calculated using readily available climate data namely the solar irradiance (S; W/m^2) and air temperature (T_a; °C) as:

$$R_n = (1 - \alpha)S + (\varepsilon_a - \varepsilon_s)\sigma(T_a + 273.15)^4, \tag{4}$$

where α is the surface albedo; and ε_a and ε_s are the emissivities of the atmosphere and surface, respectively; and σ is the Stefan-Boltzmann constant (W/(m^2·K^4)). Comparison between the modelled net radiation with that measured by net radiometers at the flux towers showed large differences. Likely sources of error for this term resided with the albedo and emissivity calculations given that S and T_a used in this study were measured on site and the sensors were calibrated regularly. So, we adopted alternative expressions for the simulated emissivities (Table 2) which have been used elsewhere in seasonally dry climates (Carrasco and Ortega-Farias, 2007; Dzikiti et al., 2014). Accurate n simulations are also critical for the PT-JPL model. In the current MOD16 model, the available energy at the plant canopies (A_c) and the soil surface (A_{soil}) are calculated as linear functions of the fractional vegetation cover (Mu et al., 2007, 2011). In this study, we adopted a Beer's law approach (Table 2) in which net radiation extinction decreased exponentially with LAI, consistent with numerous other studies (Fisher et al., 2008; Garcia et al., 2013; El Masri et al.,

2019).

Sensitivity tests were performed by varying the parameters in the MOD16 model over the range ±30% of the values (Mu et al., 2011) for specific biomes to establish parameters that had the largest impact on ET. Parameters linked to the transpiration sub-model had the largest effect on ET. In the present version of MOD16 (Mu et al., 2011), the surface conductance to transpiration ($C_s=1/r_s$) is constrained only by climatic stress factors namely the minimum air temperature (T_{min}) and the vapour pressure deficit of the air (VPD)

$$C_s = C_L \times f(T_{min}) \times f(\text{VPD}) , \qquad (5)$$

where C_L is the mean stomatal conductance per unit leaf area. Full expressions for the stress factors $f(T_{min})$ and $f(\text{VPD})$, which take values between 0 and 1, are shown in Table 2. Sensitivity tests showed that T_{min}, based on the values proposed by Mu et al. (2011) did not have any effect on ET. For this reason, we replaced the current minimum temperature based stress factor with one that uses the average air temperature (Garcia et al., 2013) (Table 2) since both the minimum and maximum air temperatures affect stomatal conductance. The VPD stress function was eliminated given that air temperature is not independent from VPD. Moreover, applying the VPD stress function (Mu et al., 2007) decreased the accuracy of the model while alternative equations use site-specific parameters (Green et al., 2003; Wever et al., 2002; Dzikiti et al., 2016).

Table 2 Proposed revisions to the MOD16 ET model using data from South African biomes

Original equation	Revised equation	
1.0 Net radiation		
(a) $\varepsilon_s = 0.97$	$\varepsilon_s = 0.95 + 0.01 \times \text{LAI}$; $\varepsilon_s=0.98$; LAI>3	Allen et al. (2002); Brutsaert (1975); Carrasco and Ortega-Farias (2007); Dzikiti et al. (2014)
(b) $\varepsilon_a = 1 - 0.26 e^{(-7.77x^{-4}xT^2)}$	$\varepsilon_a = 1.31 \times \left[\dfrac{e_a}{T_a}\right]^{\frac{1}{7}}$	
2.0 Available energy		
(a) $A_c = F_c \times A$	$A_{soil} = A e^{-k_R \times \text{LAI}} - G$	Garcia et al. (2013); Fisher et al. (2008); El Masri et al. (2019)
(b) $A_{soil} = (1 - F_c) \times A - G$	$A_c = A - A_{soil}$	
3.0 Transpiration sub-model		
(a) $f(T_{min}) = \begin{cases} 1.0, & T_{min}>T_{min\_open} \\ \dfrac{T_{min} - T_{min\_close}}{T_{min\_open} - T_{min\_close}}, & T_{min\_close}<T_{min}<T_{min\_open} \\ 0.1, & T_{min}<T_{min\_close} \end{cases}$	$f(T) = 1.1814\left[1 + e^{0.2(T_{opt}-10-T_a)}\right]^{-1}$ $\times \left[1 + e^{0.3(-T_{opt}-10-Ta)}\right]^{-1}$	Garcia et al. (2013)
(b)	$f(\text{VPD}) = 1$	This study
$f(\text{VPD}) = \begin{cases} 1.0, & \text{VPD} \le \text{VPD}_{open} \\ \dfrac{\text{VPD}_{close} - \text{VPD}}{\text{VPD}_{close} - \text{VPD}_{open}}, & \text{VPD}_{open}<\text{VPD} \le \text{VPD}_{close} \\ 0.1, & \text{VPD} \ge \text{VPD}_{close} \end{cases}$		
(c) $f(\text{SWC}) = 1$	$f(\text{SWC}) = \dfrac{\text{SWC} - \text{SWC}_{min}}{\text{SWC}_{max} - \text{SWC}_{min}}$	Fisher et al. (2008); this study
(d) $f_{wet} = \text{RH}^4$	$f_{wet} = \text{RH}^{10}$	Marsh et al. (2013); this study

Note: The original equations are sourced from Mu et al. (2011). ε_s, emissivity of the ground surface; ε_a, emissivity of atmosphere; LAI, leaf area index; e_a, actual vapour pressure of air; T_a, mean daily air temperature; A_c, available energy at the canopy level; F_c, fractional vegetation cover (equal to FPAR in Mu et al. (2011)); A_{soil}, available energy at soil surface; k_R, extinction coefficient for net radiation (equal to 0.6 (Impens and Lemeur, 1969)); G, soil heat flux; T_{min_open}, minimum temperature for stomatal opening; T_{min}, minimum temperature; T_{min_close}, minimum temperature for stomatal closure; VPD, vapor pressure deficit ; VPD_{open}, minimum vapor pressure deficit required for stomata to open; VPD_{close}, maximum vapor pressure deficit for stomatal closure; SWC, soil water content; SWC_{min}, minimum soil water content; SWC_{max}, maximum soil water content at field capacity for specific sites; f_{wet}, relative surface wetness; T_{opt}, optimum temperature for plant growth (25°C); RH, measured relative humidity.

Despite the fact that soil water deficit influences transpiration, MOD16 does not directly account for this variable. We therefore propose a simple soil water stress function, i.e., $f(\text{SWC})$ in Table 2,

principally to illustrate that the accuracy of MOD16 can significantly be improved by accounting for soil water deficit in seasonally arid ecosystems. A component-by-component inspection of the ET predictions revealed that simulated night time ET was significantly higher than the measured values. We traced this to very high values of the relative surface wetness (f_{wet}) which is calculated as the fractional relative humidity raised to the fourth power (Table 2). According to Fisher et al. (2008), the relative surface wetness represents the fraction of time when the surface is wet. A slight modification to this expression (Table 2) improved the night time ET predictions.

In the PT-JPL model, actual ET is calculated as the sum of canopy transpiration (λE_c), soil evaporation (λE_s) and wet canopy evaporation (λE_w) wherein

$$\begin{cases} \lambda E = (1 - f_{wet}) \times f_g \times f_T \times f_M \times \alpha_{PT} \times \dfrac{\Delta}{\Delta + \gamma} \times R_{nc} \\ \lambda E_s = (f_{wet} + f_{SM})(1 - f_{wet}) \times \alpha_{PT} \times \dfrac{\Delta}{\Delta + \gamma} \times (R_{ns} - G) \ , \\ \lambda E_w = f_{wet} \times \alpha_{PT} \times \dfrac{\Delta}{\Delta + \gamma} \times R_{nc} \end{cases} \qquad (6)$$

where f_{wet} is the relative surface wetness; f_g is the green canopy fraction; f_T is an air temperature constraint; f_M is the empirical factor used as a proxy for plant; α_{PT} is the Priestley-Taylor coefficient considered equal to 1.26 assuming large uniform fetch with no advection of energy at each site (Priestley and Taylor, 1972); R_{nc} is the net radiation absorbed by the canopy (W/m^2); f_{SM} is the empirical factor used as a proxy for soil water stress; R_{ns} is the net radiation absorbed by the soil (W/m^2); and G is the soil heat flux (W/m^2). Full equations for these variables are defined in Fisher et al. (2008), Garcia et al. (2013) and Ershadi et al. (2014). In this study, simulations were ran first with the original model as published (Fisher et al., 2008) and then with the soil water stress function (f_{SM}) replaced with the one proposed in Table 2.

3 Results

3.1 Microclimates and evapotranspiration (ET)

Main drivers of ET are plant and soil characteristics and the atmospheric evaporative demand. At Skukuza, for example, the green vegetation cover, and hence ET, showed clear seasonal trends in response to rainfall. We used the NDVI as a proxy for vegetation greenness and this peaked at about 0.8 in 2010 and 0.7 in 2011 (Fig. 2a). The corresponding maximum LAI was about 2.4 in 2010 and 1.9 in 2011. The dry winter season (May–August) had the lowest canopy cover as most of the species were deciduous (NDVI, 0.2) with the average LAI less than 0.2. Rainfall distribution during the summer was highly uneven at Skukuza (Fig. 2b) in both years and this accordingly affected canopy cover and ultimately ET. The long mid-summer dry spells between December and March to early April of the next year resulted in substantial declines in the soil water content (Fig. 2b), causing marked decreases in measured ET (Fig. 2c). The dry spells were so severe that the vegetation condition declined as evidenced by the reduced mid-summer NDVI (Fig. 2a) and the NDVI increased again when the rains resumed. Field capacity for soils at 50 mm depth at Skukuza, estimated from the volumetric soil water content of the probes 24 h after a heavy rain event, was around 0.12 cm^3/cm^3 while the lowest soil water content measured in the two years was around 0.05 cm^3/cm^3.

Vegetation cover at the broad leaf deciduous site at Malopeni was sparse compared to Skukuza (Fig. 3a) culminating in lower ET rates. In addition, the trees shed their leaves in winter which further lowered the ET rates. At Malopeni the NDVI was about 0.3 in winter peaking at around 0.7 in mid-summer. The corresponding LAI varied from 0.3 to a maximum of about 1.6 for the winter and summer seasons, respectively. Rainfall from March 2009 to February 2010 was 368 mm at Malopeni (Fig. 3b). The mid-summer dry spells were not very clear at Malopeni because the data were not available for the period December 2009 to February 2010 due to the equipment failure.

The field capacity of the soils at Malopeni (0.18 cm^3/cm^3) was higher than that at Skukuza while the lowest measured soil water content during the dry season was around 0.02 cm^3/cm^3. The daily maximum ET was 3.60 mm at Malopeni in 2010 (Fig. 3c), which was lower than the 5.00 mm recorded at Skukuza in the same year.

Rain falls during the winter months at Elandsberg (May–September) because the study site has a Mediterranean climate. At the other two study sites (i.e., Skukuza and Malopeni), rain falls during the summer months (Oct–March). The lowest NDVI was about 0.35 in summer and peaked at 0.60 in early spring (September 2013) (Fig. 4a). The MODIS derived LAI ranged from 0.5 in autumn (April 2013) to a maximum of 1.1 recorded in spring. This agreed with the data measured using the leaf area meter (LAI-2000, Li-COR, Inc., Nebraska, USA) at the site (Dzikiti et al., 2014). Annual rainfall at Elandsberg was 700 mm, higher than those at the other two sites (Fig. 4b). Because of the predominantly sandy soils at this site, field capacity was less than 0.10 cm^3/cm^3 while the lowest measured soil water content was around 0.03 cm^3/cm^3. Maximum daily ET (around 4.5 mm; Fig. 4c) was between those measured at Skukuza and Malopeni.
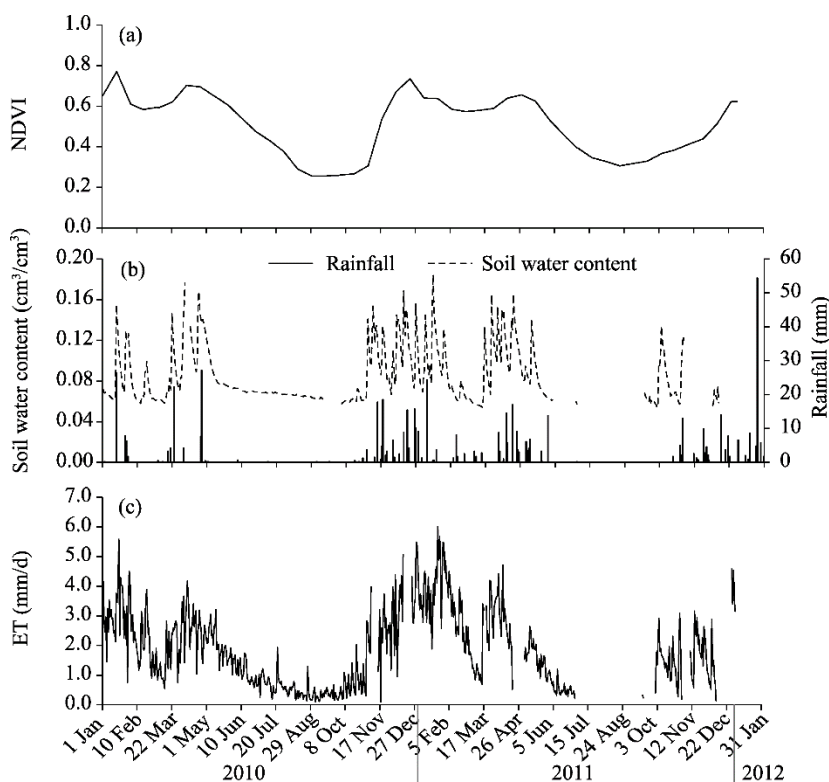

Fig. 2   Variations in NDVI (a), soil water content and rainfall (b), and measured daily evapotranspiration (ET) (c) at the deciduous needle leaf forest site at Skukuza from 1 January 2010 to 31 December 2011

Annual reference evapotranspiration (ET_0) exceeded rainfall at all sites (Table 3). ET_0 was calculated using the modified PM equation as the ET from a short grass surface that is healthy, actively growing, uniformly covering the ground and not short of water according to Allen et al. (1998). Skukuza experienced drought over the two years of the study, receiving an average rainfall of 323 mm compared to the long term average of around 547 mm. The wet and dry episodes during periods of active plant transpiration presented an ideal opportunity to test the models. The ET_0 (1090.0 mm) was more than three times higher than the rainfall at Skukuza while the measured average annual ET for 2010–2011 was approximately 610.0 mm. Elandsberg annual ET_0 was 1012.0 mm and the measured ET was about 586.0 mm. The ET_0 at Skukuza was higher than at Elandsberg as a result of the relatively warm and dry winters at Skukuza compared to Elandsberg which received rainfall in winter. It was not possible to derive the total ET for Malopeni due to the
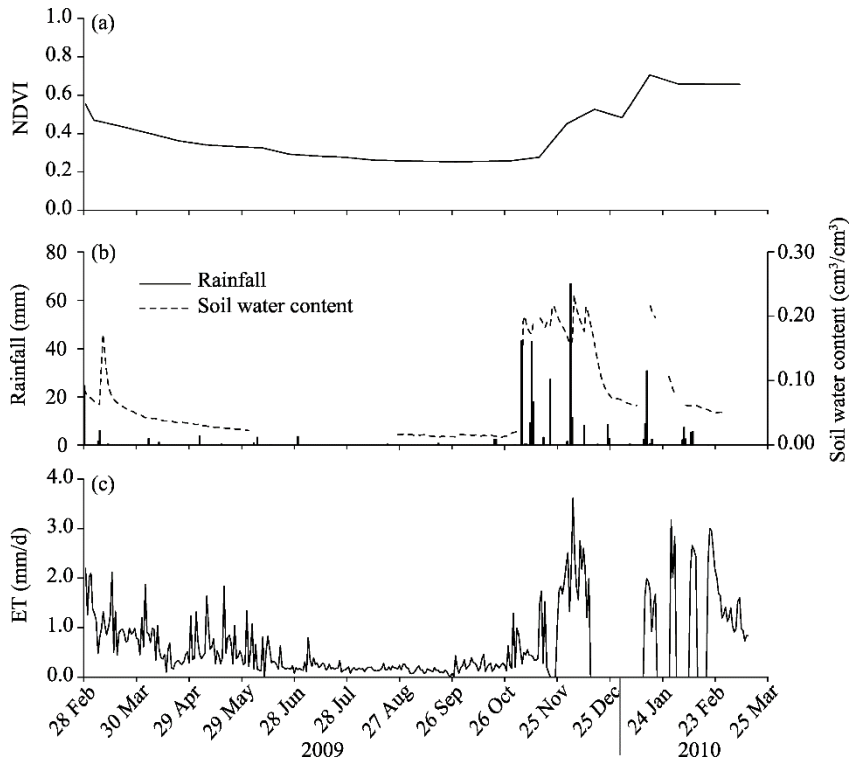
Fig. 3   Changes of NDVI (a), soil water content and rainfall (b) and measured ET (c) at the deciduous broad leaf site at Malopeni from 28 February 2009 to 14 March 2010
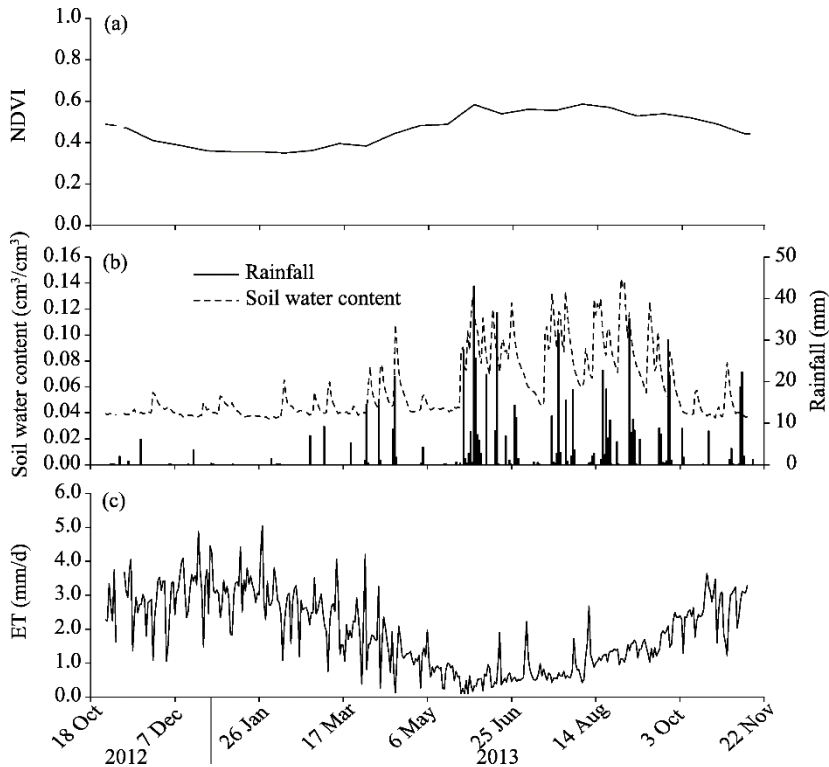

Fig. 4   Changes of NDVI (a), soil water content and rainfall (b) and ET (c) at the shrubby fynbos site at Elandsberg from 26 November 2012 to 17 October 2013

Table 3   Monthly mean daily maximum temperature (T_{max}), monthly mean daily minimum temperature (T_{min}), reference evapotranspiration (ET_0) and rainfall (P) at Skukuza, Malopeni and Elandsberg derived for the periods indicated in Table 1

Month	Skukuza				Malopeni				Elandsberg			
	T_{max}	T_{min}	ET_0	P	T_{max}	T_{min}	ET_0	P	T_{max}	T_{min}	ET_0	P
	(°C)	(°C)	(mm/d)	(mm)	(°C)	(°C)	(mm/d)	(mm)	(°C)	(°C)	(mm/d)	(mm)
Jan	28	18	104	43	38	17	-	57	40	11	156	1
Feb	29	19	110	21	38	16	-	9	40	12	117	9
Mar	29	19	97	35	38	13	98	33	42	13	105	15
Apr	25	15	78	36	36	10	76	4	37	8	60	62
May	25	11	67	11	37	9	59	4	32	1	30	46
Jun	23	4	60	0	35	6	49	5	26	2	26	186
Jul	20	6	59	0	33	5	51	4	27	2	35	91
Aug	22	7	75	1	36	7	69	1	29	3	46	135
Sept	27	13	99	12	38	13	80	2	28	4	66	87
Oct	32	15	108	25	39	15	103	7	37	13	107	55
Nov	31	16	112	55	41	14	109	121	36	8	114	9
Dec	30	17	122	84	39	16	-	121	39	13	150	4
Total	na	na	1091	323	na	na	na	368	na	na	1012	700

Note: -, data not available; na, not applicable.

missing data (Fig. 3c). The low correlation between the measured daily ET and the atmospheric evaporative demand, depicted by the ET_0, suggests that climatic factors were not the only major drivers of ET at the summer rainfall sites (Figs. 5a and b). Soil water deficit was indeed an important driver of ET at Skukuza given the clear responses to dry spells and the same can be said for actual Malopeni (Figs. 2b and c). At Elandsberg however, there was a linear relationship between the ET and ET_0 (Fig. 5c) with the ET to ET_0 ratio of approximately 0.58. This suggested that climatic conditions were the main drivers of ET at the winter rainfall site.
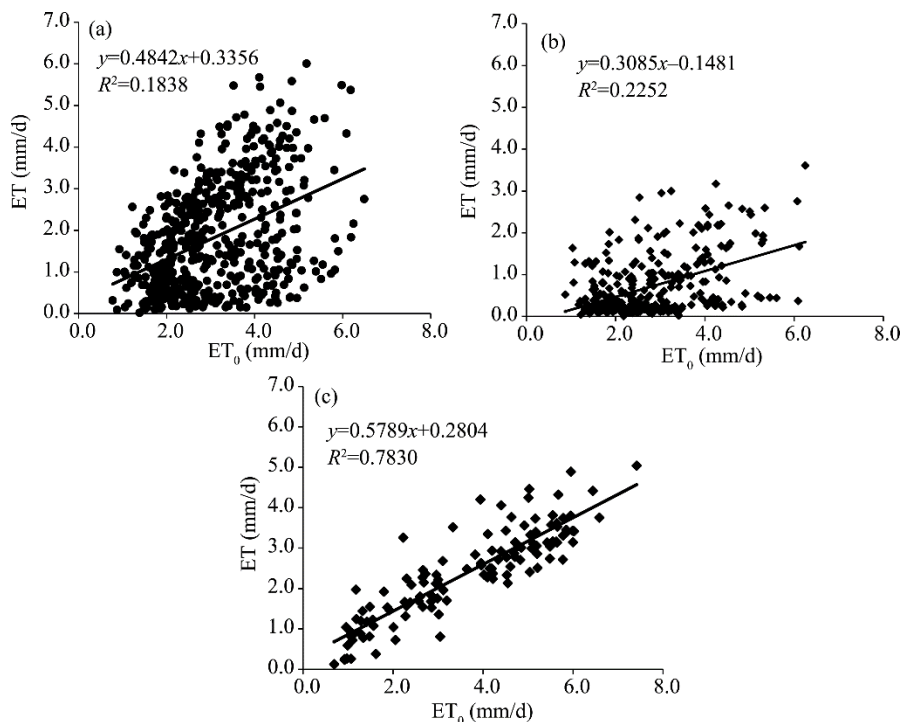
Fig. 5   Effects of the atmospheric evaporative demand, depicted by the reference evapotranspiration (ET_0) on the actual evapotranspiration at Skukuza (a), Malopeni(b) and Elandberg (c)

The vegetation at Elandsberg likely had access to water from the saturated zone given that the water levels were quite shallow (<4 m) and this may have reduced the impact of the soil water deficit on ET.

3.2   Model simulations and sensitivity tests

Comparisons between the measured and MOD16 modelled daily net radiation for the Skukuza and Malopeni sites combined (Fig. 6a) showed substantial differences of up to 26%. Negative daily net radiation values were predicted on some overcast days. Predictions of the daily total ET from all the three sites by the original MOD16 (Mu et al., 2011) and PT-JPL models are shown in Figures 6b and c, respectively. Both models clearly underestimated the daily ET especially at high values. For MOD16, this is consistent with the results from recent studies, e.g., Ramoelo et al. (2014) and Tang et al. (2015). The MOD16 root mean square error (RMSE) values were 1.17, 0.53 and 1.46 mm/d for Skukuza, Malopeni and Elandsberg, respectively (Table 4). For the PT-JPL model, the RMSE values were 1.19, 0.76, and 1.26 mm/d for the above three sites, respectively.
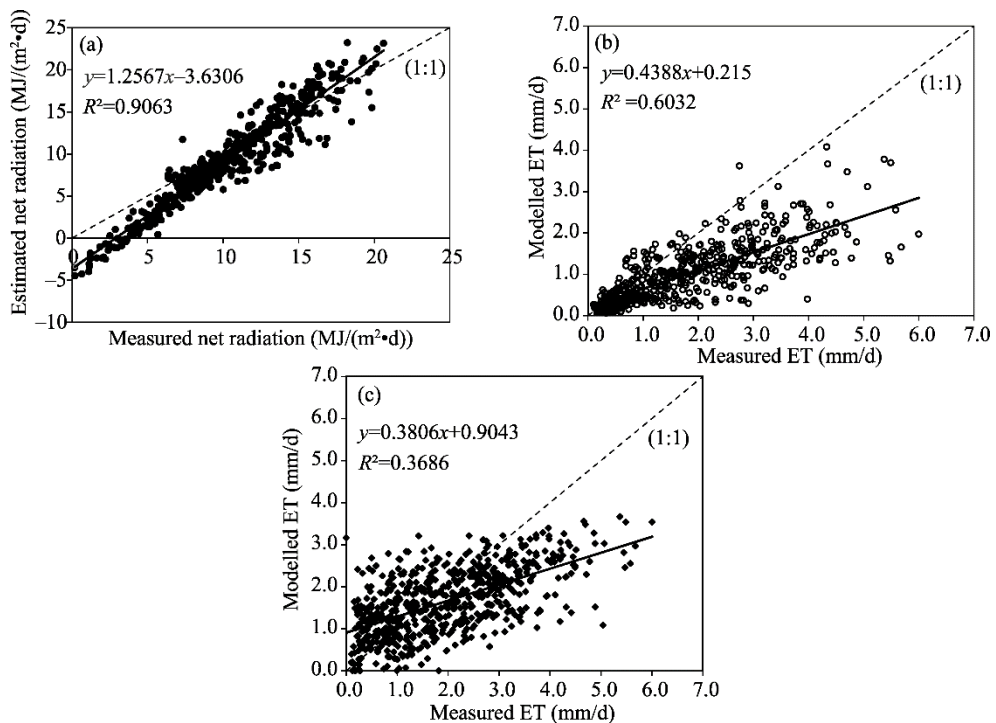

Fig. 6   Relationships between the measured and MOD16 modelled daily net radiation (a), the measured and MOD16 modelled daily evapotranspiration (b), and the measured and PT-JPL modelled daily ET (c) using combined data for the Skukuza and Malopeni sites, respectively

The proposed changes in the radiation balance sub-model are shown in Table 2, and there is an improved match between the measured and modelled net radiation in Figure 7 compared to the original relationship in Figure 4a. In addition, biome specific mean stomatal conductance per unit leaf area (C_L) values were also derived based on the results of a sensitivity test which showed that this parameter had the largest influence on the modelled ET.

Derivation of the C_L values was achieved by inverting the PM equation and using the measured values of the latent heat flux, soil heat flux, net radiation, wind speed, VPD and LAI (Zhang et al., 1997) collected over a period of one week during active transpiration periods and when the vegetation was not under water stress. This yielded C_L values were 0.0051, 0.0042 and 0.0065 m/s for Skukuza, Malopeni and Elandsberg, respectively. An illustration of the day/night partitioning of ET by MOD16 over a 16-d period at Skukuza (1–16 January 2011) after implementing the suggested changes (Fig. 8). The measured night time ET was less than 10% of the measured daily total ET and this was reasonably well predicted by the model (Fig. 8).

Table 4 Performance of the original and revised versions of the MOD16 and Priestley-Torr (PT-JPL) models using daily ET data from Skukuza, Malopeni and Elandsberg

Model	Site	Slope	Intercept	R^2	RMSE (mm/d)	MAE (mm/d)
	Skukuza	0.44	0.22	0.60	1.17	0.86
MOD16	Malopeni	0.50	0.17	0.47	0.53	0.31
	Elandsberg	0.30	0.25	0.52	1.46	1.23
	Skukuza	0.31	1.24	0.23	1.19	0.97
PT-JPL	Malopeni	0.43	1.17	0.23	0.78	0.64
	Elandsberg	0.43	0.42	0.39	1.26	0.97
	Skukuza	0.86	0.15	0.76	0.55	0.48
Revised MOD16	Malopeni	0.82	0.11	0.73	0.39	0.28
	Elandsberg	0.76	0.95	0.52	0.57	0.48
	Skukuza	0.63	0.44	0.62	0.68	0.49
Revised PT-JPL	Malopeni	1.36	−0.14	0.62	0.84	0.40
	Elandsberg	0.66	1.37	0.40	1.12	0.91

Note: RMSE, root mean square error; MAE, mean absolute error of the simulations. Modelled data are the dependent variables while the measured data are the independent variables.
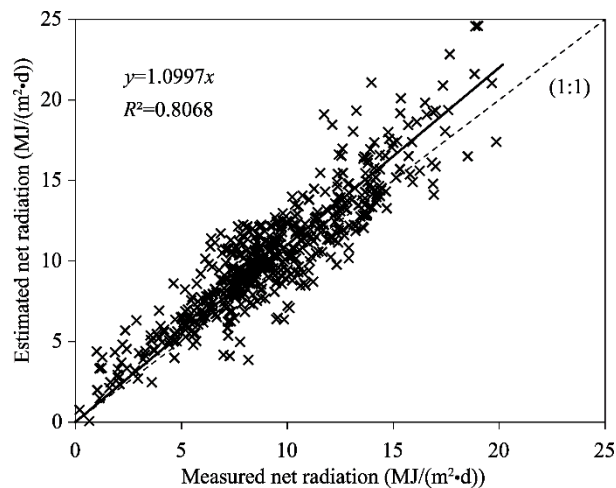
Fig. 7 Simulation of the net radiation with the improved radiation budget (Eq. 4)
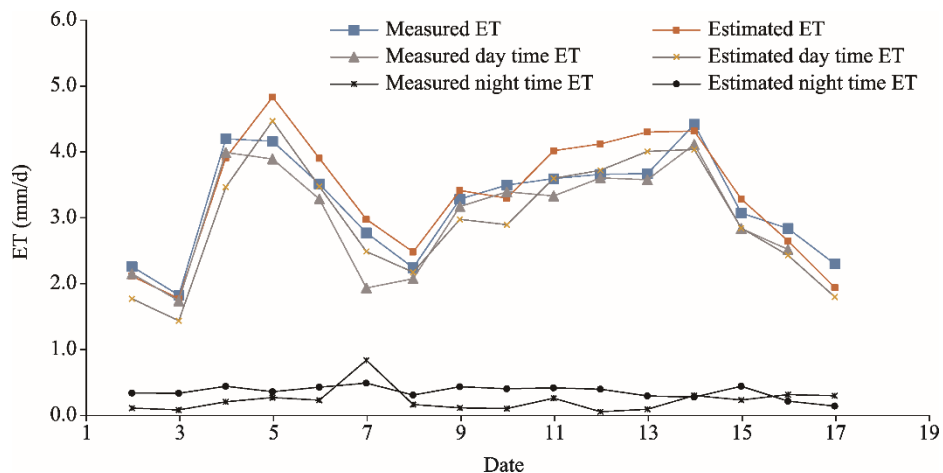
Fig. 8 Day and night time partitioning of the ET during summer from 2 to 17 January 2011 at Skukuza simulated using the modified MOD16 model

Daily total ET over the study period at the three sites were also well predicted by the revised MOD16 (Fig. 9). In particular, mid-summer dry spells at Skukuza (Fig. 9a) and Malopeni (Fig. 9b) were also accurately captured and this did not happen when soil water deficit was not incorporated into the model. Implementing the revised PT-JPL yielded some improvements to the ET simulations (Fig. 10) but these were less significant than those realised with MOD16. As shown in Table 4, the RMSE values for the revised MOD16 ET were 0.55, 0.39 and 0.57 mm/d for Skukuza, Malopeni and Elandsberg, respectively, while the PT-JPL had RMSE values of 0.68, 0.84 and 1.12 mm/d, respectively.
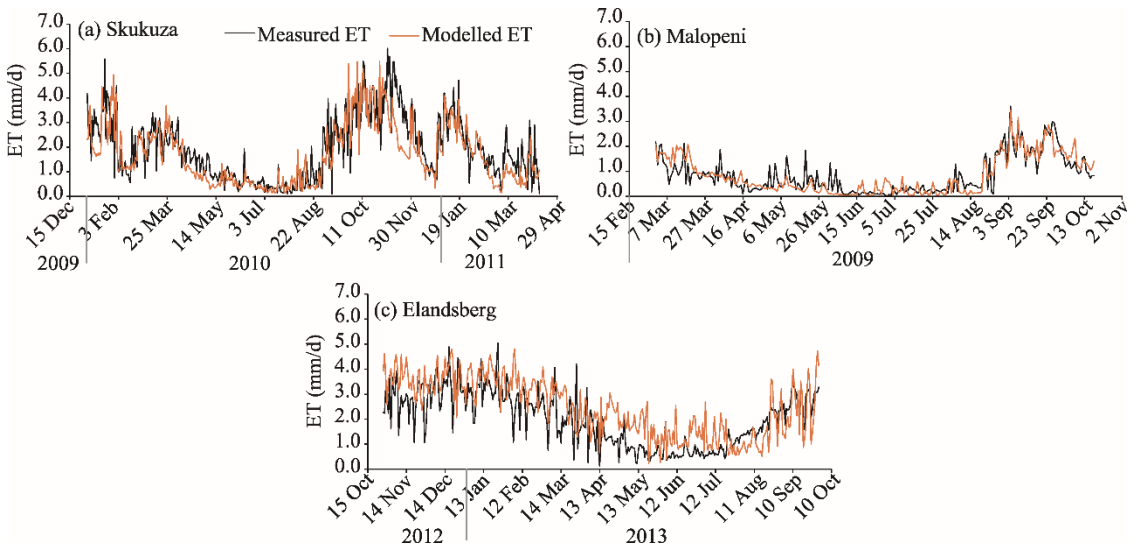

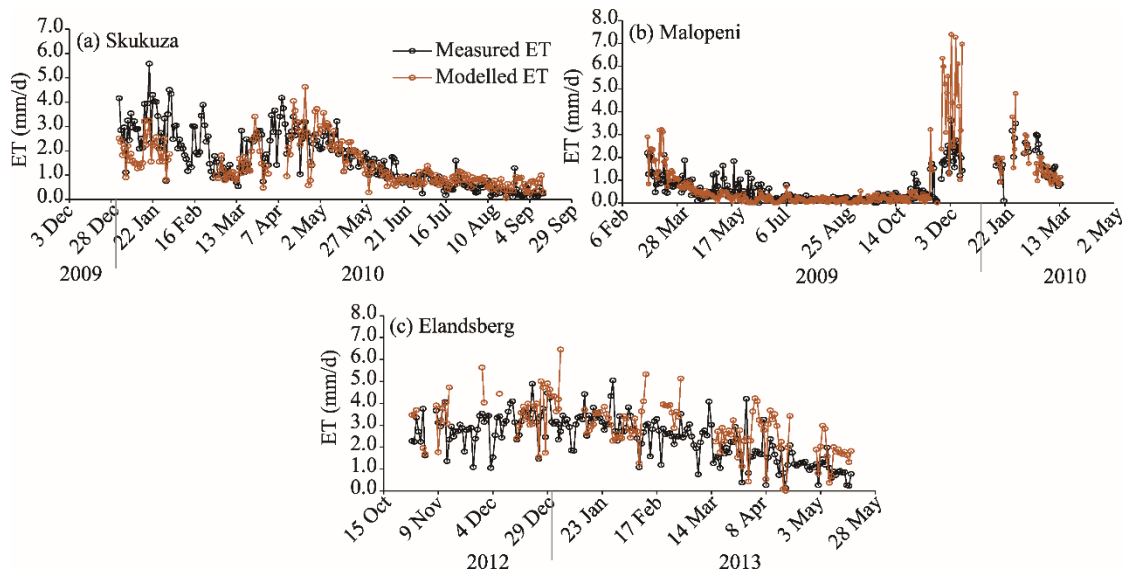**Fig. 9** Measured and modelled daily ET with the modified MOD16 model at Skukuza (a), Malopeni (b) and Elandsberg (c)

Fig. 10 Measured and modelled daily ET with the modified PT-JPL model at Skukuza (a), Malopeni (b) and Elandsberg (c)

4   Discussion

The MOD16 algorithm by Mu et al. (2011) was developed for global ET estimates. It is expected

that the uncertainties may be high in the model predictions at specific locations. Validation at local sites is therefore imperative for informed decision making, e.g., by water resources managers, irrigators and in climate change studies. Up to date, MOD16 has been validated using point data from flux towers at various locations in Asia (Kim et al., 2012), the USA (Velpuri et al., 2013) and Africa (Ramoelo et al., 2014). While accurate ET predictions have been observed at some sites, uncertainties as high as 50%–60% have also been reported elsewhere (Kim et al., 2012; Velpuri et al., 2013). Some studies noted the inconsistent performance by MOD16 between years using data from the same sites with accurate predictions in some years (Ramoelo et al., 2014). In this study, we evaluated the performance of MOD16 together with another widely used ET model, PT-JPL using data from dry ecosystems with different characteristics and with simulations done at the daily time step. In general, the uncertainties in ET predictions using remote sensing models are the highest under these two scenarios (Garcia et al., 2013; Velpuri et al., 2013). This study therefore provided an opportunity to identify possible sources of error and to suggest ways to improve the parameterization of the models in arid environments.

The original MOD16 and PT-JPL models both underestimated the daily ET at all three sites in South Africa (Fig. 3). Similar performances were observed with the PT-JPL in arid environments (Garcia et al., 2013; Marshall et al., 2013) and these authors suggested various changes to the model. One reason for the failure of MOD16 to accurately predict the daily ET especially at the summer rainfall sites was the occurrence of prolonged mid-summer dry spells during active transpiration periods which caused significant soil water deficits. This in turn led to substantial ET reductions (Fig. 2c) due to stomatal closure under severe water stress. Because transpiration has the largest contribution to total ET during peak vegetation cover (Mu et al., 2011), significant errors are likely with the current MOD16 in which transpiration is constrained only by climatic factors. The fact that the vegetation at Elandsberg had other sources of water other than soil water led to smaller improvements in the simulated ET when soil water deficit was incorporated in the algorithms. Our data demonstrates that using representative values of the mean stomatal conductance per unit leaf area for each biome and implementing a soil water stress constraining function to the transpiration sub-model in MOD16 can significantly improve the performance of this model in seasonally arid environments. Sensitivity tests revealed that a 30% change in a key biophysical inputs such as the LAI caused up to 21% change in the ET estimated by MOD16. Hwang and Choi (2013) evaluated the previous MOD16 model (Mu et al., 2007) and observed that a 17%–20% change in net radiation yielded up to 20% change in ET. This observation also supports our findings wherein an improvement in the net radiation simulations significantly improved the ET estimates.

To operationally implement the soil water stress function within the MOD16 framework, considerable works are still required particularly to identify an accurate remote sensing based soil water content product whose data is readily available. In a similar study at two Mediterranean ecosystems, Garcia et al. (2013) observed improved ET simulations with the PT-JPL model by incorporating a soil water stress function which was based on the calculation of the apparent thermal inertia of the soil (Verstraeten et al., 2006). The thermal inertia concept is based on the fact that increasing soil water content modifies the thermal conductivity of the soil and it also reduces the diurnal temperature fluctuation (Price, 1977). They used 15 min land surface temperature data derived from the Meteosat Second Generation and surface albedo from MODIS. In this study however, incorporating a soil water stress function based on the actual measured soil water content data (i.e., replacing f_{SM} in Eq. 6 with f(SWC) in Table 2) did not significantly improve the performance of the PT-JPL model at all the three sites. Another source of error with MOD16 was the estimation of the night time ET. Simulated night time ET was up to 60% higher than the measured values and this was a result of over estimates in the relative surface wetness which was derived using the expression proposed by Fisher et al. (2008), i.e., relative humidity to the fourth power (RH^4). Reducing the relative surface wetness by using RH^{10} improved the prediction of the night time ET. Marshall et al. (2013) made a similar observation with the PT-JPL model at various semi-arid sites across Africa.

5 Conclusions

This study evaluated two widely used remote sensing ET models using data from highly dynamic semi-arid environments characterized by rapid fluctuations in the soil water content during peak plant water use periods. It is clear from our assessment that significant improvements to the MOD16 algorithm are possible in semi-arid ecosystems by (1) implementing accurate mean stomatal conductance per unit leaf area for each respective biome; (2) incorporating a soil water stress function in the transpiration sub-model to capture transpiration reductions due to soil water deficits; (3) improving the parameterization of the radiation balance sub-model; and (4) correctly estimating the relative surface wetness especially for night time ET simulations. However, the lack of reliable and readily available sources of remotely sensed soil water content data still remains a major challenge for the implementation of these changes. The lack of a credible soil water constraint in MOD16 likely contributes to the often observed good performance of the model in humid environments or in wet years when soil water deficit does not limit ET and poor simulations in dry ecosystems or during dry spells. Further researches are therefore required to identify accurate soil water content products that can be incorporated into the MOD16 framework. The apparent thermal inertia concept (Price, 1977; Verstraeten et al., 2006; Garcia et al., 2013) is a promising idea, but this still needs more validation. High temporal resolution soil moisture mapping using upcoming satellite products such as Sentinel as proposed by Paloscia et al. (2013) also provide opportunities for improving remote sensing ET models. While less input data intensive ET models like the PT-JPL have yielded promising results elsewhere, improved parameterization is needed to increase their accuracy in arid and semi-arid ecosystems.

Acknowledgements

References

Allen R G, Pereira L S, Raes D, et al. 1998. Crop evapotranspiration - Guidelines for computing crop water requirements - FAO Irrigation and drainage paper No.56. FAO. Rome, Italy.

Brutsaert W. 1975. On a derivable formula for long-wave radiation from clear skies. Water Resources Research, 11(5): 742–744.

Burba G G, Verma S B. 2005. Seasonal and interannual variability in evapotranspiration of native tallgrass prairie and cultivated wheat ecosystems. Agricultural and Forest Meteorology, 135(1–4): 190–201.

Carrasco M, Ortega-Farias S. 2007. Evaluation of a model to simulate net radiation over a vineyard cv. Cabernet Sauvignon. Chilean Journal of Agricultural Research, 68: 156–165.

Cleugh H A, Leuning R, Mu Q Z, et al. 2007. Regional evaporation estimates from flux tower and MODIS satellite data. Remote Sensing of Environment, 106(3): 285–304.

Cleverly R W, Bistrow J W. 1979. Revised volcanic stratigraphy of the Lebombo monocline. South African Journal of Geology, 82(2): 227–230.

Dzikiti S, Jovanovic N Z, Bugan R, et al. 2014. Measurement and modelling of evapotranspiration in three fynbos vegetation types. Water SA, 40(2): 189–198.

Dzikiti S, Gush M B, Le Maitre D C, et al. 2016. Quantifying potential water savings from clearing invasive alien *Eucalyptus camaldulensis* using *in situ* and high resolution remote sensing data in the Berg River Catchment, Western Cape, South Africa. Forest Ecology and Management Journal, 361: 69–80.

Dzikiti S, Volschenk T, Midgley S J E, et al. 2018. Estimating the water requirements of high yielding and young apple orchards in the winter rainfall areas of South Africa using a dual source evapotranspiration model. Agricultural Water Management. 208: 152–162.

El Masri B, Rahman A F, Dragoni D. 2019. Evaluating a new algorithm for satellite-based evapotranspiration for North American ecosystems: Model development and validation. Agricultural and Forest Meteorology, 268: 234–248.

Ershadi A, McCabe M F, Evans J P, et al. 2014. Multi-site evaluation of terrestrial evaporation models using FLUXNET data. Agricultural and Forest Meteorology, 187: 46–61.

Fisher J B, Tu K P, Baldocchi D D. 2008. Global estimates of the land-atmosphere water flux based on monthly AVHRR and ISLSCP-II data, validated at 16 FLUXNET sites. Remote Sensing of Environment, 112(3): 901–919.

Garcia M, Sandholt I, Ceccato P, et al. 2013. Actual evapotranspiration in drylands derived from in-situ and satellite data: Assessing biophysical constraints. Remote Sensing of Environment, 131: 103–118.

Garcia M, Fernández N, Villagarcía L, et al. 2014. Accuracy of the temperature-vegetation dryness index using MODIS under water-limited vs. energy-limited evapotranspiration conditions. Remote Sensing of Environment, 149: 100–117.

Green S, McNaughton K, Wünsche J N, et al. 2003. Modelling light interception and transpiration of apple tree canopies. Agronomy Journal, 95(6): 1380–1387.

Hwang K Choi M. 2013. Seasonal trends of satellite-based evapotranspiration algorithms over a complex ecosystem in East Asia. Remote Sensing of Environment, 137: 244–263.

Impens I, Lemeur R. 1969. Extinction of net radiation in different crop canopies. Theoretical and Applied Climatology, 17: 403–412.

Kim H W, Hwang K, Mu Q, et al. 2012. Validation of MODIS 16 global terrestrial evapotranspiration products in various climates and land cover types in Asia. KSCE Journal of Civil Engineering, 16(2): 229–238.

Low A B, Rebelo A G. 1996. Vegetation of South Africa, Lesotho and Swaziland. Pretoria: Department of Environmental Affairs and Tourism of South Africa.

Makarau A, Jury M R. 1997. Seasonal cycles of convective spells over Southern African during austral summer. International Journal of Climatology, 17(2): 1317–1333.

Marshall M, Tu K, Funk C, et al. 2013. Improving operational land surface model canopy evapotranspiration in Africa using a direct remote sensing approach. Hydrology and Earth System Sciences, 17: 1079–1091.

Monteith J L, Unsworth M H. 1990. Principles of Environmental Physics. Oxford: Butterworth Heinemann Press, 1–291.

Mu Q M, Heinsch F A, Zhao M S, et al. 2007. Development of a global evapotranspiration algorithm based on MODIS and global meteorology data. Remote Sensing of Environment, 111(4): 519–536.

Mu Q M, Zhao M S, Running S W. 2011. Improvement to a MODIS global terrestrial evapotranspiration algorithm. Remote Sensing of Environment, 115(8): 1781–1800.

Mu Q M, Zhao M S, Running S W. 2013. MOD16 1-km^2 terrestrial evapotranspiration (ET) product for the Nile Basin algorithm theoretical basis document. In: Numerical Terradynamic Simulation Group College of Forestry and Conservation University of Montana. Missoula, USA.

Mucina J L, Rutherford M C, Leslie W P, et al. 2006. The Vegetation of South Africa, Lesotho and Swaziland. Pretoria: South African National Biodiversity Institute, 1–807.

Műnch Z, Conrad J E, Gibson L A, et al. 2013. Satellite earth observation as a tool to conceptual hydrological fluxes in the Sandveld, South Africa. Hydrology Journal, 21(5): 1053–1070.

Nishida K, Nemani R R, Glassy J M, et al. 2003. Development of an evapotranspiration index from Aqua/MODIS for monitoring surface moisture status. IEEE Transactions on Geoscience and remote sensing, 41(2): 493–501.

Paloscia S, Pettinato S, Santi E, et al. 2013. Soil moisture mapping using Sentinel-1 images: Algorithm and preliminary validation. Remote Sensing of Environment, 134: 234–248.

Polhamus A, Fisher J B, Tu K P. 2013. What controls the error structure in evapotranspiration models? Agricultural and Forest Meteorology, 169: 12–24.

Price J C. 1977. Thermal inertia mapping: A new view of the earth. Journal of Geophysical Research, 82(18): 2582–2590.

Priestley C H B, Taylor R J. 1972. On the assessment of surface heat flux and evaporation using large scale parameters. Monthly Weather Review, 100(2): 81–92.

Ramoelo A, Majozi N, Mathieu R, et al. 2014. Validation of global evapotranspiration product (MOD16) using flux tower data in the African Savannah, South Africa. Remote Sensing, 6(8): 7406–7423.

Reinders F B. 2013. Irrigation methods for efficient water application: 40 years of South African research excellence. Water SA, 37(5): 765–770.

Ruhoff A L, Paz A R, Aragao L E O C, et al. 2013. Assessment of the MODIS global evapotranspiration algorithm using eddy covariance measurements and hydrological modelling in the Rio Grande basin. Hydrological Sciences Journal, 58(8): 1658–1676.

Savage M J, Everson C S, Odhiambo G O, et al. 2004. Theory and practice of evapotranspiration measurement, with special focus on surface layer scintillometer (SLS) as an operational tool for the estimation of spatially-averaged evaporation. In: Water Research Commission Report No 1335/1/04, Implementation of Bichromatic Scintillation as an Operational Tool for the Estimation of Spatially Averaged Evaporation. Pretoria, South Africa.

Scholes R J, Gureja N, Giannecchinni M, et al. 2001. The environment and vegetation of the flux measurement site near Skukuza,

Kruger National Park. Koedoe, 44(1): 73–83.

Schulze R E, Maharaj M, Warburton M L, et al. 2008. South African atlas of climatology and agrohydrology. In: Water Research Commission Report No 1489/1/08. Pretoria, South Africa.

Talsma C J, Good S P, Jimenez C, et al. 2018. Partitioning of evapotranspiration in remote sensing based models. Agricultural and Forest Meteorology, 260–261: 131–143.

Tang R, Shao K, Li Z, et al. 2015. Multiscale Validation of the 8-day MOD16 Evapotranspiration Product Using Flux Data Collected in China. IEEE Journal of Selected Topics in Applied Earth Observations and Remote Sensing, 8(4): 1478–1486.

Velpuri N M, Senay G B, Singh R K, et al. 2013. A comprehensive evaluation of two MODIS evapotranspiration products over the conterminous United States: Using point and gridded FLUXNET and water balance ET. Remote Sensing of Environment, 139: 35–49.

Verstraeten W W, Veroustraete F, van der Sand C J, et al. 2006. Soil moisture retrieval using thermal inertia, determined with visible and thermal spaceborne data, validated for European forests. Remote Sensing of Environment, 101(3): 299–314.

Waters R, Allen R, Tasumi M, et al. 2002. Surface energy balance algorithms for land: Advanced training and users manual. The Idaho Department of Water Resources. Idaho, USA.

Wever L A, Flanagan L B, Carlson P J. 2002. Seasonal and interannual variation in evapotranspiration, energy balance and surface conductance in a northern temperate grassland. Agricultural and Forest Meteorology, 112(1): 31–49.

Yao Y J, Liang S L, Cheng J, et al. 2013. MODI-driven estimation of terrestrial latent heat flux in China based on a modified Priestley-Taylor algorithm. Agricultural and Forest Meteorology, 171–172: 187–202.

Yao Y J, Liang S L, Li X L, et al. 2015. A satellite-based hybrid algorithm to determine the Priestley-Taylor parameter for global terrestrial latent heat flux estimation across multiple biomes. Remote Sensing of Environment, 165: 216–233

Zhang D, Zhang Q, Werner A D, et al. 2016. Assessment of the reliability of popular satellite products in characterizing the water balance of the Yangtze River Basin, China. Hydrology Research 47 (S1): 8–23.

Zhang H P, Simmonds L P, Morison J I L, et al. 1997. Estimation of transpiration by single trees: comparison of sap flow measurements with a combination equation. Agricultural and Forest Meteorology, 87(2–3): 155–169.

Zhang Y Q, Chiew F H S, Zhang L, et al. 2008. Estimating catchment evaporation and runoff using MODIS leaf area index and the Penman-Monteith equation. Water Resources Research, 44(10): W10420.